Journal of Power Sources 196 (2011) 1358–1364

Contents lists available at ScienceDirect

Journal of Power Sources

journal homepage: www.elsevier.com/locate/jpowsour

Electrical and electrochemical studies of poly(vinylidene fluoride)–clay nanocomposite gel polymer electrolytes for Li-ion batteries

M. Deka, A. Kumar*

Materials Research Laboratory, Department of Physics, Tezpur University, Assam 784028, India

ARTICLE INFO

Article history:
Received 26 June 2010
Received in revised form 30 August 2010
Accepted 10 September 2010
Available online 22 September 2010

Keywords:
Polymer–clay nanocomposite
Gel polymer electrolyte
Impedance spectroscopy
Ionic conductivity
Lithium-ion battery

ABSTRACT

A study is conducted on the electrical and electrochemical properties of nanocomposite polymer electrolytes based on intercalation of poly(vinylidene fluoride) (PVdF) polymer into the galleries of organically modified montmorillonite (MMT) clay. A solution intercalation technique is employed for nanocomposite formation with varying clay loading from 0 to 4 wt.%. X-ray diffraction results show the β phase formation of PVdF on intercalation. Transmission electron microscopy reveals the formation of partially exfoliated nanocomposites. The nanocomposites are soaked with 1 M $LiClO_4$ in a 1:1 (v/v) solution of propylene carbonate (PC) and diethyl carbonate (DEC) to obtain the required gel electrolytes. The structural conformation of the nanocomposite electrolytes is examined by Fourier transform infrared spectroscopy analysis. Examination with a.c. impedance spectroscopy reveals that the ionic conductivity of the nanocomposite gel polymer electrolytes increases with increase in clay loading and attains a maximum value of 2.3×10^{-3} S cm^{-1} for a 4 wt.% clay loading at room temperature. The same composition exhibits enhancement in the electrochemical and interfacial properties as compared with that of a clay-free electrolyte system.

1. Introduction

Polymer electrolytes have attracted world-wide attention because they combine high ionic conductivity with solid, yet flexible, mechanical properties for application in various electrochemical devices, particularly in solid-state rechargeable lithium batteries [1]. Such batteries are expected to offer safe and reliable performance for both hybrid electric vehicles and domestic applications. Nevertheless, the most widely studied poly(ethylene oxide) (PEO) based solid polymer electrolytes complexed with lithium salts have not yet been used for practical applications because they possess very low ionic conductivity (10^{-7} to 10^{-8} S cm^{-1}) at ambient temperature [2], despite a high solvating power for lithium salts and compatibility with lithium electrode [3]. On the other hand, plasticized or gel polymer electrolytes (GPEs) have high ambient temperature ionic conductivity by immobilizing a large amount of liquid electrolyte in the polymer host [4]. The conductivity and mechanical stability of GPEs are mutually exclusive, i.e., the ionic conductivity in GPEs increases at the expense of reduced mechanical strength, and vice versa [5]. Moreover, leakage of organic liquid solvents from the polymer electrolyte is yet another problem for GPEs when used in a device over a long period of time. This leakage leads to a decrease in ionic conductivity with damage to the lithium electrode and other components. Fortunately, these problems can be effectively circumvented by uniform dispersion of nano or submicron-sized inorganic fillers in the polymer matrix and it has been shown that fillers may influence greatly the properties of polymer electrolytes [6].

Nanocomposites based on polymer/layered silicates are promising new material systems with structural and functional advantages over conventionally reinforced polymers [7,8]. Among the most commonly used inorganic layered hosts, montmorillonite (MMT) is a favoured choice in view of its special features of high aspect ratio (~1000), high cation-exchange capacity (CEC ~80 mequiv./100 g), large specific surface area (~31.82 m^2 g^{-1}), and appropriate interlayer charge (~0.55) and length scale (clay channel width = 16 Å). Typically, the chemical structures of montmorillonite (MMT) consist of two fused silica tetrahedral sheets that sandwich an edge-shared octahedral sheet of either magnesium or aluminum hydroxide. The Na^+ and Ca^{2+} residing in the interlayer regions can be substituted by organic cations such as alkylammonium ions by a cationic-exchange reaction to render the hydrophilic-layered silicate organophilic. Intercalating polymer in the layered host can produce a polymer nanocomposite electrolyte with a huge interfacial area. A higher interfacial area not only sustains the mechanical properties of PVdF-based gel polymer electrolytes, but also increases the solubility of lithium salts due to higher dielectric property [9]. Recently, many related investigations have reported the use of polymer/clay nanocomposites in solid-state electrolytes, where the intercalated or exfoliated state of MMT plays an important role in ion conduction in these electrolytes [10,11]. Additionally, the dispersion of nanolayers of

* Corresponding author. Tel.: +91 3712267007; fax: +91 3712267006.
E-mail address: ask@tezu.ernet.in (A. Kumar).

0378-7753/$ – see front matter © 2010 Elsevier B.V. All rights reserved.
doi:10.1016/j.jpowsour.2010.09.035

mineral clay was found to enhance the thermal stability, mechanical strength, molecular barrier and flame-retardant properties of polymers [12–15].

In the present work, an investigation is conducted on the electrical and electrochemical properties of PVdF based nanocomposite gel polymer electrolytes using MMT as fillers, $LiClO_4$ as salts and (PC + DEC) as a plasticizer, with a view to enhancing the ion transport, electrochemical and interfacial stabilities, and gain an understanding of the mechanism of the processes.

2. Experimental

2.1. Materials

Poly(vinylidene fluoride) (PVdF, Sigma–Aldrich, M_w = 2 75 000), propylene carbonate (PC, E-Merck, Germany), diethyl carbonate (DEC, E-Merck, Germany), lithium perchlorate ($LiClO_4$, Sigma–Aldrich) were vacuum dried prior to use. 25–30 wt.% octadecylamine modified montmorillonite clay (MMT) (Sigma–Aldrich) was used as a nanoclay. Tetrahydrofurane (THF, E-Merck, Germany) and other analytical grade reagents were used without purification.

2.2. Preparation of nanocomposites and gel polymer electrolytes

Different amounts of modified MMT (1, 2.5 and 4 wt.%) were dispersed in 5 ml of THF by ultrasonication. The dispersed MMT solution was then mixed with PVdF solution (15% solid content (w/v) in DMSO) by mechanical stirring at 50 °C followed by ultrasonication for 30 min. The nanocomposite films were obtained by a solution casting method and dried under vacuum at room temperature. The dried films were denoted as PVdF1, PVdF2.5 and PVdF4 and correspond to a nanoclay loading of 1, 2.5 and 4 wt.%, respectively.

The nanocomposite gel polymer electrolytes were prepared by immersing the films in a liquid electrolyte solution containing 1 M $LiClO_4$ in PC:DEC = 1:1 (v/v), for a period of 10 h. The films swell quickly, and the percentage of solution uptake was calculated using the relation:

$$\text{Uptake}\,(\%) = \frac{W_t - W_0}{W_0} \times 100 \quad (1)$$

where W_t and W_0 are the weights of the wet and dry films, respectively. The nanocomposite gel polymer electrolytes were denoted as gel PVdF, gel PVdF1, gel PVdF2.5 and gel PVdF4 which correspond to the gel for pure PVdF, PVdF1, PVdF2.5 and PVdF4 nanocomposites.

2.3. Analysis and characterization techniques

X-ray diffraction patterns of the prepared films were obtained with a Rigaku miniflex diffractometer at room temperature. The distribution of the clay layers was studied with transmission electron microscopy (TEM). The ionic conductivities of the nanocomposite polymer electrolyte films were determined by a.c. impedance measurements using a Hioki 3532-50 LCR HiTester in the frequency range from 42 Hz to 5 MHz. A two-electrode system was employed for ionic conductivity measurements, wherein the polymer electrolyte membrane was inserted between the two stainless-steel electrodes. An a.c. sinusoidal signal of 3 mV with varying frequencies was applied across the cell and the impedance modulus and phase shift of the electrode|electrolyte|electrode cell assembly were measured. The temperature dependence of ionic conductivity was also measured by heating the samples from room temperature (25 °C) to 90 °C. The nature of the conductivity of the nanocomposites gel polymer electrolytes was determined by transference number measurements using the Wagner polarization technique with the polymer electrolyte films held between graphite blocking electrodes. The transference number is found to be ≈0.97, which indicates that conductivity is essentially ionic in nature. The interfacial stability of nanocomposite polymer electrolytes was studied by fabricating Li|polymer electrolyte|Li cells at room temperature and was monitored for 20 days. The anodic decomposition voltage was determined by linear sweep voltammetry by using an electrochemical workstation (Sycopel AEW 2, UK). Fourier transform infrared spectroscopy (FTIR) was conducted with a Nicolet Impact 410 (Madison, USA) unit using KBr pellets.

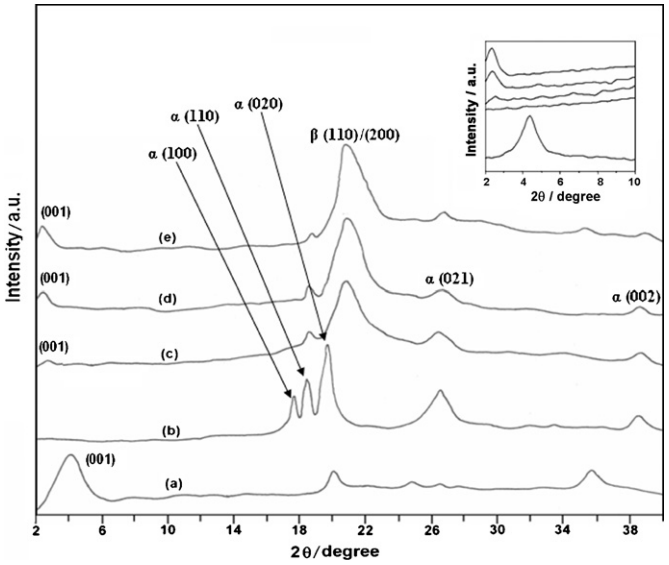

Fig. 1. XRD patterns (a) pure organophilic MMT, (b) pure PVdF, (c) PVdF1, (d) PVdF2.5 and (e) PVdF4. Inset shows reflection of (0 0 1) in range 2θ = 2–10°.

3. Results and discussion

3.1. X-ray diffraction analysis

The X-ray diffraction (XRD) patterns of pure MMT, pure PVdF and PVdF/MMT nanocomposites with different wt.% of MMT loading are shown in Fig. 1. Pure MMT exhibits a (0 0 1) diffraction peak at 2θ = 4.4° (Fig. 1a) corresponding to an interlayer spacing of 2 nm, while the same peak is shifted to 2θ = 2.55, 2.4 and 2.35°, corresponding to an interlayer spacing of 3.46, 3.65 and 3.75 nm for 1, 2.5 and 4 wt.% clay loading in the nanocomposites, respectively. The gallery spacing increases by more than 1 nm in the nanocomposites as compared with that for pure MMT exhibiting intercalation of polymer chains inside the galleries of layered silicate. At a low clay content (1 wt.%), the intercalation of the polymer leads to the disordering of the layered clay structure and thereby a decrease in the XRD scattering intensity, as shown in Fig. 1c. The nanocomposite containing 1 wt.% clay content demonstrates both exfoliation and intercalation properties. With the further addition of clay, the intensity of the d_{001} peak increases, indicating intercalation of the polymer in the layers without disruption of the ordered structure [16]. The intensity of the (0 0 1) diffraction peaks for 2.5 and 4 wt.% clay loading, however, is low compared with that of pure MMT and this suggests that some clay layers still exist in the form of exfoliated nanostructures.

Pure PVdF exhibits characteristic peaks at 2θ values of 17.8, 18.6 and 20°, corresponding to (1 0 0), (1 1 0) and (0 2 0) reflections, respectively. These three peaks are attributed to the α phase of PVdF [17]. With the addition of clay to PVdF, the peaks at 17.8 and 20° due to the α phase diminish, whereas the intensity of the peak at 18.6° decreases significantly. On the other hand, one new peak at

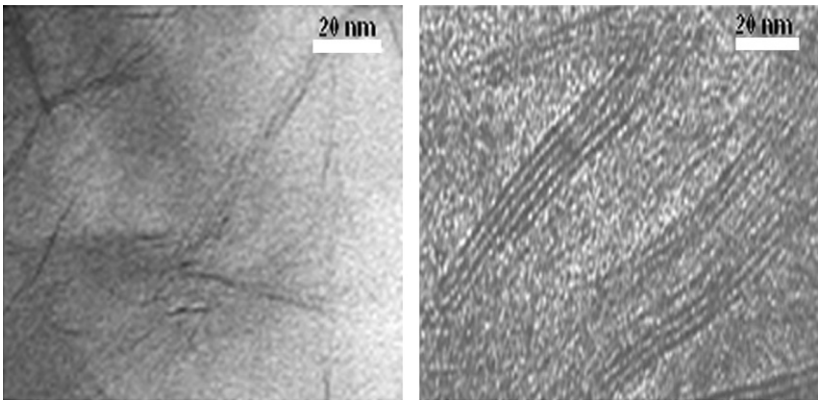

Fig. 2. TEM image of PVdF/MMT nanocomposite with (a) 1 and (b) 4 wt.% organophilic MMT.

20.6° is observed in the composites, which could be attributed to unresolved (1 1 0) and (2 0 0) reflections of the β phase of PVdF [17]. Thus the addition of MMT clays to PVdF leads to the formation of the β phase. The α and β-phases of PVdF have TGTG/ and TT molecular conformations, respectively [18]. The TGTG/ conformation of the α phase is known to be the most common and more thermodynamically stable phase than the TTTT conformation of the β phase of PVdF. The β-phase can be induced by several techniques, the most common being the mechanical stretching of the α-phase films at a suitable temperature [19]. In the present case, the α to β phase formation of PVdF upon inclusion of MMT can be explained on the basis of the stretching of PVdF chains during intercalation into the galleries of MMT. Thermodynamically, a decrease in the Gibbs free energy (ΔG) is required for the overall intercalation process. The driving force for direct polymer intercalation from solution is the entropy gained by desorption of solvent molecules, which compensates for the entropy decrease of confined, intercalated chains [20]. On the other hand, the conformational energy cost of stretching the chains resulting in the formation of β phase, in addition to the topographical constrains and the adsorption on the surfaces, are expected to impose severe limitations on the diffusion of chains in a pseudo two-dimensional slit. The α phase peaks (0 2 1) ($2\theta = 26.4°$) and (0 0 2) ($2\theta = 38.5°$) obviously decrease in intensity suggesting that MMT clays disturb the ordered structure perpendicular to the planes (0 2 1) and (0 0 2).

As polymer intercalates into the galleries of MMT, a significant compressive strain is expected in MMT layers. The strain arises due to the dislocation of the ordered clay layers from their original crystal structure as a result of insertion of polymer chains into the galleries. The strain has been calculated quantitatively for (0 0 1) reflection of MMT by employing a single-line profile analysis using the Voigt function [21]. This procedure involves the extraction and analysis of Gaussian (β_G) and Lorentzian (β_L) components of integral breadth of a single Bragg peak corrected for instrumental broadening. After correcting the instrumental broadening, the remaining line broadening (β) is believed to be due to crystallite size (β_{cryst}) and retained strain (β_{strain}) broadening [22]. Therefore,

$$\beta = \beta_{cryst} + \beta_{strain} \quad (2)$$

$$\text{and} \quad \varepsilon = \frac{\beta_{strain}}{4 \tan\theta} \quad (3)$$

The microstrain calculated for pure MMT is 0.155, which increases with the addition of MMT clay and becomes 0.213, 0.242 and 0.275 for PVdF1, PVdF2.5 and PVdF4, respectively. It is known that the intercalation of PVdF chains into the interlayer galleries depend on the concentration of clay and polymer [16]. With increase of clay loading in the PVdF matrix, more polymer chains go into the galleries resulting in a significant increase of compressive strain. The increased strain causes the MMT layers, to exfoliate, which results in decreased X-ray peak intensity and increased peak broadening as observed in Fig. 1.

3.2. TEM analysis

The partial exfoliated structure of the clay layers in the nanometer range can be observed from the TEM image (Fig. 2). The distribution pattern of the clay layers inside the matrix (PVdF1 and PVdF4) is seen in the picture. For PVdF1 (Fig. 2a), most of the clay layers are well dispersed and are found to be disordered in a random fashion in the PVdF matrix. This indicates that the extent of exfoliation is more than that of intercalation in case of PVdF1. On the other hand, the micrograph of PVdF4 (Fig. 2b) exhibits mostly intercalated morphology with well diffused clay layers in the polymer chains. Thus TEM results corroborate the XRD results.

3.3. Swelling behaviour of nanocomposites

The major difference between gel polymer electrolytes and solid polymer electrolytes lies in the presence of plasticizer in the polymer system [4]. The dynamic swelling behaviour of PVdF and PVdF–clay nanocomposite films in 1 M $LiClO_4$ containing a 1:1 (v/v) ratio of plasticizers PC and DEC at room temperature is shown in Fig. 3. PC has a high dielectric constant ($\varepsilon = 64.6$) and a high viscosity ($\eta = 2.53$), whereas DEC has a low dielectric constant ($\varepsilon = 2.82$)

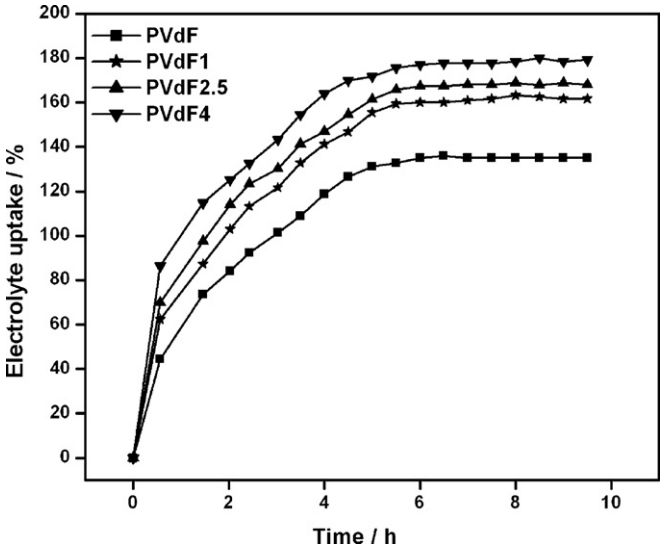

Fig. 3. Swelling behaviour of PVdF and PVdF/MMT nanocomposites.

and low viscosity ($\eta = 0.748$). A combination of PC and DEC (1:1, v/v) solvents was used as an optimization for a high dielectric constant ($\varepsilon = 33.71$) and low viscosity ($\eta = 1.639$) to achieve high ionic conductivity. It is observed from Fig. 3 that the % of swelling or solvent uptake as calculated using Eq. (1) for both PVdF and PVdF–clay nanocomposites increases with increase of the soaking period up to 6 h. The increase in the % of swelling for nanocomposites is more than that for pure PVdF for an equal soaking time with weight uptake ratios of 130, 160 and 169% for pure PVdF, PVdF1 and PVdF2.5, respectively. In addition, solvent uptake of the polymer film containing 4 wt.% of clay shows the highest % of swelling (177%) compared with the other nanocomposite films and this indicates the capacity of MMT clays to facilitate solvent uptake. The increase of electrolyte absorption is a result of the excellent affinity of nanoclays towards polar PC/DEC molecules (solvent of the electrolyte). Moreover, the high aspect ratio of nanoclays enhance the retention of electrolyte solution in the composite films and thereby leads to enhancement in ionic conductivity of PVdF–clay nanocomposites, as discussed in next section.

3.4. Ionic conductivity measurements

Typical Nyquist plots of PVdF and PVdF/MMT nanocomposite gel polymer electrolyte films at room temperature are shown in Fig. 4. All plots comprise a semicircular arc in the high-frequency region and an oblique line in the low-frequency region. This response of the electrode|electrolyte|electrode cell assembly can be simulated as an equivalent circuit comprising a combination of a bulk resistance 'R_b' of the sample in parallel with its geometrical capacitance 'C_g' in series with a constant-phase element (CPE) that consists of a double-layer interfacial capacitor C_{dl} and a charge-transfer resistance [23]. The total impedance of the equivalent circuit at a frequency ω can be written as:

$$Z_{Total} = \left[\frac{1}{1+(\omega R_b C_g)^2}\right] - jR_b\left[\frac{\omega R_b C_g}{1+(\omega R_b C_g)^2}\right] + \frac{1}{\omega C_{dl}} \quad (4)$$

At high frequencies when the reactance and the bulk resistance of the sample are comparable i.e., $1/\omega C_g \approx R_b$, a parallel combination of bulk resistance R_b and capacitance C_g contributes dominantly to the overall impedance and gives rise to a semicircle [23]. At low frequencies when $1/\omega C_g \leq R_b$, the contribution of C_g becomes negligible to the overall impedance and the equivalent circuit behaves as a series combination of R_b and a constant-phase element giving an inclined spike displaced by R_b on the abscissa of the impedance plot. Inset of Fig. 4 shows the equivalent circuit for the impedance spectra obtained in this study. The impedance of CPE is given by:

$$Z_{CPE} = k(j\omega)^{-p} \quad \text{where } 0 < p < 1 \quad (5)$$

When $p = 0$, Z is frequency independent and k is just the resistance. When $p = 1$, $Z = k/j\omega = -j/\omega(k)$, the constant k^{-1} now corresponding to the capacitance. When p is between 0 and 1, the CPE acts in a way that is intermediate between a resistor and a capacitor. The series CPE terms tilt the spike and parallel CPE terms broaden the semicircle [24].

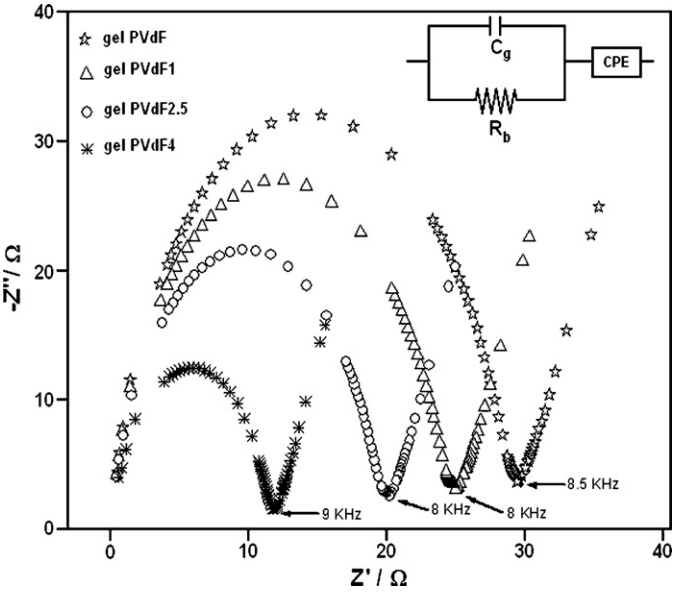

Fig. 4. Nyquist plots of gel PVdF and PVdF/MMT nanocomposite gel polymer electrolytes at different clay loadings. Inset shows equivalent circuit representing actual cell assembly.

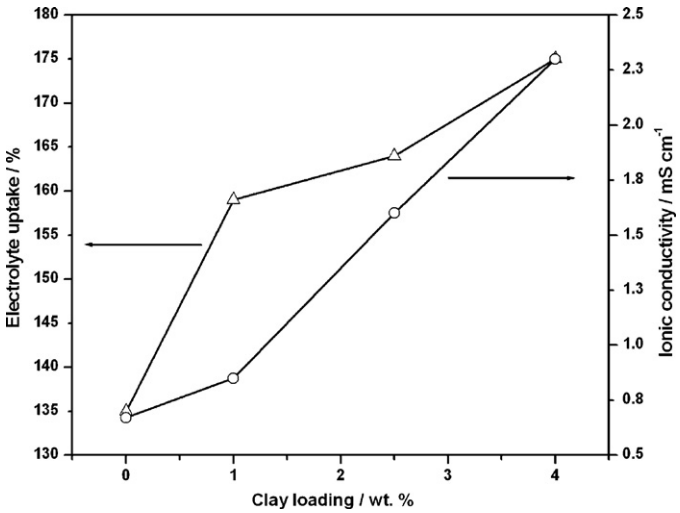

Fig. 5. Ionic conductivity (right ordinate) and electrolyte uptake (left ordinate) of nanocomposite gel polymer electrolytes as function of organophilic MMT.

From the above discussion, it is clear that the high-frequency semicircle can be ascribed to the bulk of polymer electrolytes, whereas the low-frequency spike is due to the capacitance of the electric double-layer formed at the electrode|electrolyte interface. The bulk resistance (R_b) is determined from the intercept of the semicircular arc with the abscissa. The conductivity, σ, can be obtained from $\sigma = l/R_b A$, where l is the thickness of the polymer electrolyte film and A its area. The ionic conductivity increases with increase in clay loading and attains a maximum value of 2.3×10^{-3} S cm^{-1} at room temperature for 4 wt.% clay content, see Fig. 5. It is worth mentioning that above 4 wt.% of clay loading, the polymer nanocomposite films become brittle and it is difficult for brittle films to be used in battery fabrication, so the ratio of organophilic MMT to PVdF should be controlled up to 4 wt.%. The enhancement of conductivity by adding MMT to the polymer matrix is a combined effect of high aspect ratio of the MMT clay particles and the increase in uptake of liquid electrolyte into the PVdF matrix. The high aspect ratio of MMT fillers causes steric hindrance and thereby prevent polymer chains from undergoing crystallization, which favours fast ionic transport [25]. Higher uptake of liquid electrolyte by the nanocomposite films results in increase in the concentration of charge carriers for the same volume and this leads to higher ionic conductivity. The variation in ionic conductivity with electrolyte uptake is presented in Fig. 5. As discussed in Section 3.1, clay addition to α-PVdF results in the formation of β-PVdF, in which all the fluorine atoms are oriented on the same side of the chain with the hydrogen atoms on the opposite side. This change in conformation will force all the H atoms to be oriented upwards inside the gallery because of their interaction with negatively charged clay platelets. Negatively charged F-ions atoms

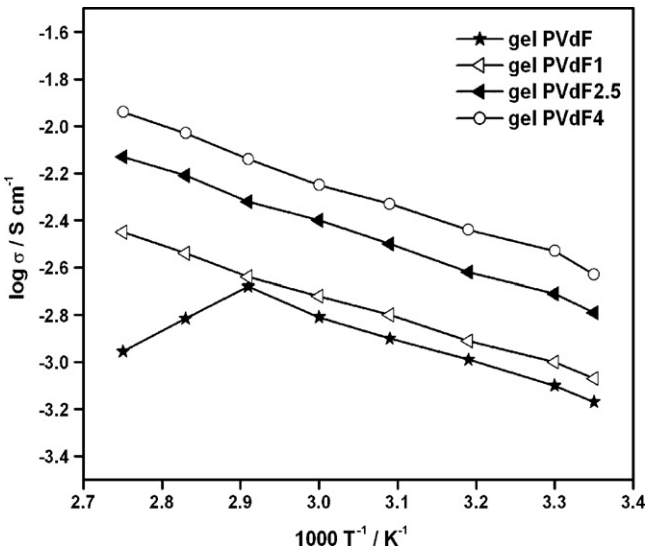

Fig. 6. Temperature dependence of ionic conductivity of gel PVdF and PVdF/MMT nanocomposite gel polymer electrolytes at different clay loadings.

will be oriented downwards and lithium ion mobility is expected to be higher along the interface lined with F atoms, which results in increase in ionic conductivity [26]. Moreover it has been reported that the enhancement of ionic conductivity in PEO-based polymer electrolytes by the addition of nanoscale inorganic oxides is not due to a corresponding increase in polymer segmental motion, but more likely a weakening of polymer–cation association induced by the nanoparticles [27]. The same effect can be applied in PVdF–clay system. If the filler–salt interaction is the major factor in determining the ionic conductivity of the composite electrolytes, we may expect that the conductivity is related to the dielectric constant of the oxide filler at the same electrolyte uptake. In the present case, MMT clay is used as inorganic filler, which is a natural mineral with a high dielectric constant [28]. The presence of high dielectric constant electronegative silicate layers in the nanocomposite could increase the dissolution of the electrolyte salt ($LiClO_4$), thereby increasing the ion conduction through the solvent domain surrounding the polymer matrix. The cationic charges on the surface of MMT act as Lewis acid centres and compete with Li^+ cations (strong Lewis acid) to form complexes with the polymer host. This, in turn, may result in: (i) structural modifications and the promotion of Li^+-conducting pathways at the surface of filler, and (ii) lowering of the ionic coupling, which promotes salt dissociation [29]. These two effects combine to increase the free ions and account for the observed enhancement in the ionic conductivity.

Fig. 6 presents the temperature dependent ionic conductivity, which follows a linear trend i.e., Arrhenius behaviour governed by:

$$\sigma = \sigma_0 \exp\left(\frac{-E_a}{kT}\right) \quad (6)$$

where σ, σ_0, E_a, k and T are the ionic conductivity, pre-exponential factor, activation energy, Boltzmann constant and absolute temperature, respectively. It has been reported [30,31] that ionic transport in gel polymer electrolytes obeys the VTF (Vogel–Tamman–Fulcher) relation $\{\sigma = B\exp(-E_a/k(T-T_0)$, where B is a constant and T_0 is the idealized glass transition temperature that is typically 20–50 K below the glass transition temperature of the polymer}, which describes the transport properties in a viscous polymer matrix [30,31]. Since the glass transition temperature (T_g) of PVdF is about −35 °C and after gelling with liquid electrolyte it is expected to drop further, T_0 is far below the region of measurement from room temperature (25 °C) to 90 °C. Therefore, VTF behaviour can be modelled as linear Arrhenius behaviour, as shown in Fig. 6. As expected, increase in temperature leads to increase in ionic conductivity due to increase in the polymer chain flexibility producing more free volume, which leads to increased polymer segmental mobility.

An interesting effect occurs in the high-temperature range wherein at about 70 °C the conductivity of the filler-free GPE dramatically decays. This is ascribed to the fact that at this temperature the polymer melts and the film loses its consistency [32]. On the other hand, the polymer–clay nanocomposite electrolytes are more stable and the conductivity continues to increasing up to 90 °C. This is attributed to the fact that the fluidity of the polymer is restricted by the presence of MMT fillers and hence the mechanical strength of the polymer electrolytes is increased and thereby are suitable materials for high-temperature operation [32].

3.5. FTIR analysis

Vibrational spectroscopy has been identified as a powerful tool to study the interactions among the various constituents in polymer electrolytes. FTIR spectra of pure PVdF and gel PVdF with different clay loading are presented in Fig. 7. Careful analysis of the FTIR spectrum of pure PVdF (Fig. 7a) suggests that the typical vibrational band observed at 1404 cm^{-1} corresponds to the deformed vibration of the CH_2 group [33]. The peak at 1233 is assigned to the –C–F– stretching mode, whereas the peaks at 1176 and 1072 cm^{-1} are due to $-C-F_2-$ stretching modes. The frequency 881 cm^{-1} corresponds to the vinylidene group of the PVdF [34]. Characteristic bands of the crystalline α-phase are observed at 763 and 615 cm^{-1}. The absorption band at 763 cm^{-1} is assigned to a rocking vibration, and that at 615 cm^{-1} to a mixed mode of CF bending and CCC skeletal vibration. The characteristics peaks of β-PVdF are observed at 834 and 510 cm^{-1}. The band at 840 cm^{-1} is ascribed to a mixed mode of CH_2 rocking and CF_2 asymmetric stretching vibration, and the band at 512 cm^{-1} to the bending mode of CF_2 [35]. It appears from Fig. 7 that as MMT content increases, the intensity of the bands at 763 and 615 cm^{-1} decrease, while that of the bands due to the β phase at 834 and 512 cm^{-1} decrease. Thus FTIR results are consistent with the XRD results discussed above.

After swelling the PVdF samples with liquid electrolytes, all the characteristics peaks of PVdF shift towards lower frequencies and thus indicate interaction among the constituents of the polymer electrolytes. The bands at 1750 and 1644 cm^{-1} (Fig. 7b) are assigned

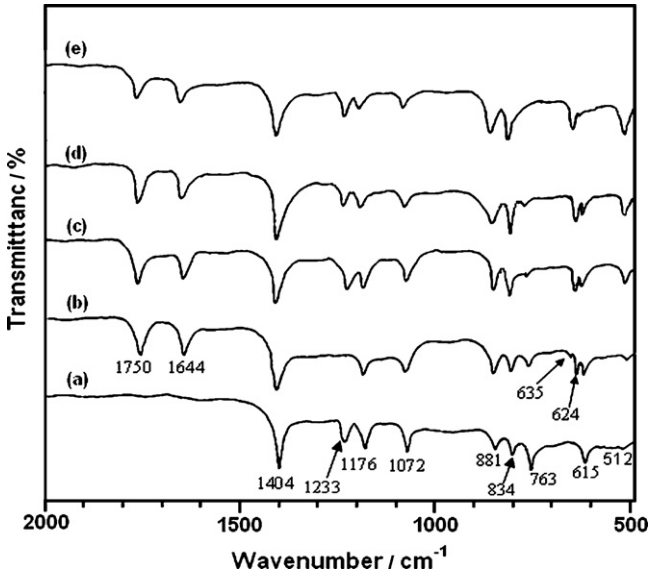

Fig. 7. FTIR spectra of (a) pure PVdF, (b) gel PVdF, (c) gel PVdF1, (d) gel PVdF2.5 and (e) gel PVdF4.

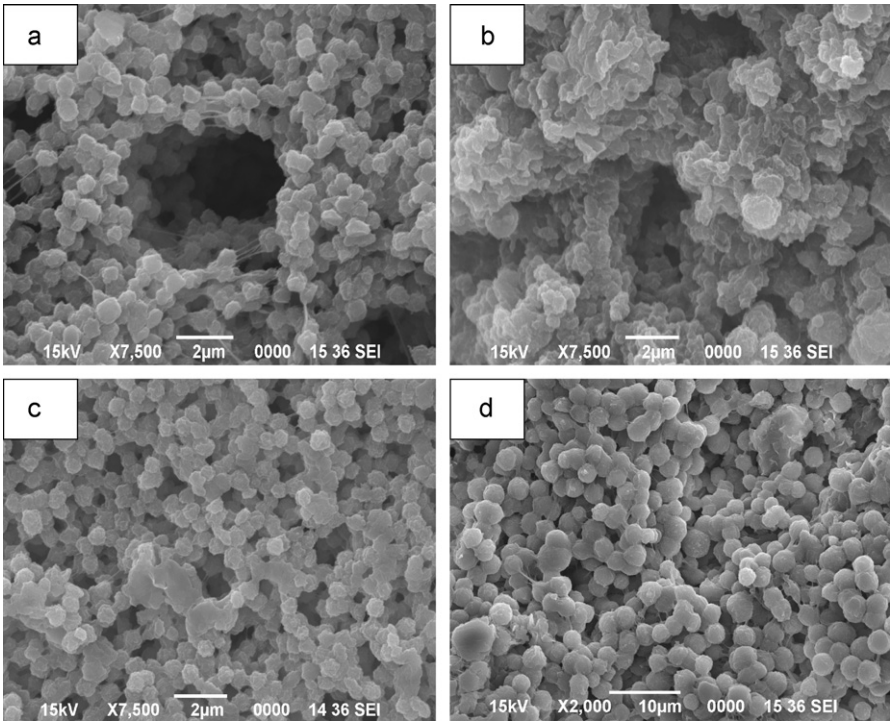

Fig. 8. SEM image of (a) gel PVdF, (a) gel PVdF1, (c) gel PVdF2.5 and (d) gel PVdF4.

to >C=O stretching vibration of plasticizer (PC + DEC) and >C=C< bonding, respectively. The $\upsilon(ClO_4^-)$ internal mode of $LiClO_4$ displays one peak at about 624 cm^{-1}, which can be assigned to the free anion that does not interact with the lithium cation, whereas the peak at 635 cm^{-1} is due to contact ion-pair formation. The peak at 635 cm^{-1} is gradually reduced to a shoulder with the addition of MMT, as shown in Fig. 7. This phenomenon may be attributed to the fact that MMT clay particles suppress the association of Li^+ and ClO_4^- ions and increase the concentration of free ions leading to an increase in the ionic conductivity.

3.6. Morphological studies

The morphology of PVdF and PVdF–MMT nanocomposite gel polymer electrolytes was examined by SEM and the results are reported in Fig. 8. Spherical granular morphology with large pores is observed in gel PVdF (Fig. 8a). The pores in the microstructure are due to solvent removal [36]. On the addition of clay to the PVdF matrix, the pore size is reduced and the surface becomes smoother as the concentration of MMT clay is increased (Fig. 8b–d). The results indicate that clay-loaded gel PVdF electrolyte systems have a higher solvent retention ability than clay-free electrolytes. In other words, the surface morphology of a nanocomposite polymer electrolyte without pores or any phase separation is indicative of a high affinity of the PVdF polymer for liquid electrolyte. The SEM results are consistent with the view that the higher conductivity of clay-loaded gel polymer electrolytes arises from increased solvent retention.

3.7. Electrochemical studies

Linear sweep voltammetry (LSV) measurements conducted using the Li|CPE|Li cell configuration for determination of the electrochemical stability window of the electrolyte systems are presented in Fig. 9. The measurements were carried out from 2 to 6 V at a scan rate 0.1 mV s^{-1}. The onset of the current identifies the anodic decomposition voltage of the electrolytes. The decomposition voltage increases with increase in clay loading and commences at about 4.6 V for a 4 wt.% clay content, as compared with 4.3 V for the clay-free electrolyte. Thus there is an improvement in the voltage stability factor in the electrolyte films containing clay. It is well known that the anodic stability window is limited by irreversible oxidation of the salt anion [37]. The Lewis acid sites on the anionic surface of MMT can interact with ClO_4^- (Lewis base), thereby enhancing the electrochemical potential window by retarding decomposition of the lithium salt anion. This working voltage range (i.e., electrochemical potential window) appears to be sufficient for application of the nanocomposite gel polymer electrolyte films as a solid-state separator/electrolyte in Li-ion batteries.

The compatibility of polymer electrolyte membranes with lithium metal is still an unsolved problem with respect to their application in high-power Li-ion batteries. The reactivity of the anode electrode with polymer electrolyte can lead to an uncon-

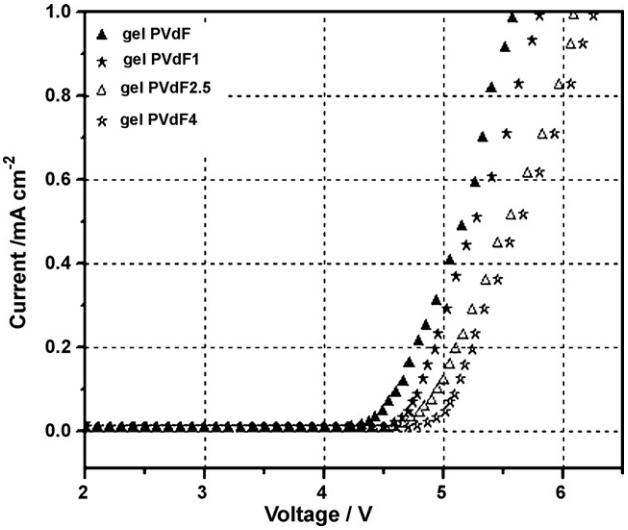

Fig. 9. Linear sweep voltammetry plots of gel PVdF and PVdF/MMT nanocomposite gel polymer electrolytes at different clay loadings.

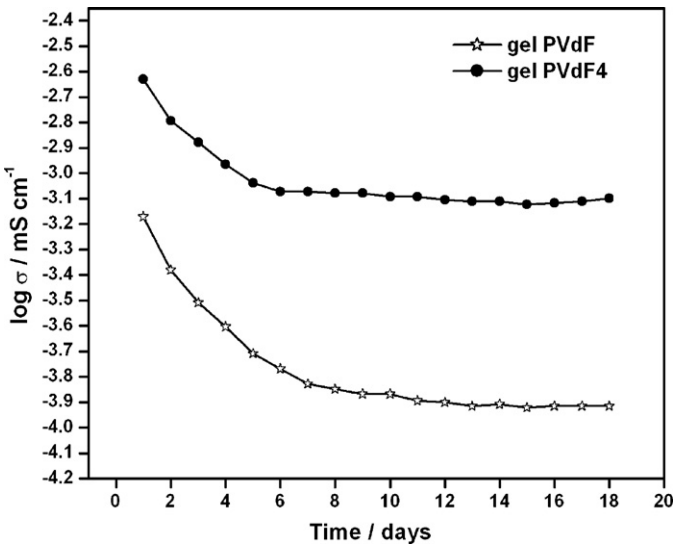

Fig. 10. Interfacial stability of gel PVdF and PVdF/MMT nanocomposite gel polymer electrolyte with 4 wt.% clay loading.

trolled passivation process and results in the formation of a thick and non-uniform surface layer [38]. These can, in turn, cause an uneven lithium deposition during the charging process and eventually lead to dendritic growth and short-circuiting of the cell [39]. Therefore, the interfacial property of lithium metal with polymer electrolytes plays a vital role in polymer Li-ion batteries for practical application. In order to examine the interfacial stability of a PVdF-based gel polymer electrolyte before and after addition of organoclay, the ionic conductivity was measured by fabricating Li|polymer electrolyte|Li cells at room temperature and monitored for 18 days. Polymer electrolytes without clay and containing 4 wt.% MMT clay have been selected to observe the effect of clay on the interfacial stability; the results are shown in Fig. 10. The ionic conductivity of both electrolytes decreases with time but the decrease in the clay-free polymer electrolyte is much larger than that in the polymer electrolyte containing MMT clay. This confirms that the interfacial stability of the polymer electrolyte containing clay is better than that of the clay-free electrolyte.

To the best of the authors' knowledge, the interfacial stability of polymer/clay nanocomposite electrolytes has not yet been reported in the literature. On the other hand, the improvement of interfacial stability in nanocomposite polymer electrolytes due to the addition of nano-sized ceramic fillers and fibres has been widely reported [32,38,29,40], according to which the high surface area of nano-sized ceramic fillers form a barrier layer at the electrode that effectively impedes the electrode–electrolyte reaction. This in turn reduces the passivation layer on the electrode and causes better interfacial stability between the electrode and the electrolyte. MMT clay is a natural mineral with a high aspect ratio and its presence in the polymer matrix prevents the electrode material from coming into direct contact with the electrolyte that protects it from passivation.

4. Conclusions

Organically modified MMT clays have been employed to modify the electrical and electrochemical properties of PVdF-based gel electrolytes. The insertion of the PVdF chain into the galleries of MMT increases the *d*-spacing from 2 to 3.75 nm for a 4 wt.% clay loading, as revealed by XRD and TEM results. Intercalation of PVdF into the galleries of MMT also results in the formation of the β phase of PVdF. Addition of clay in PVdF enhances the uptake of liquid electrolyte due to the excellent affinity of clays towards electrolyte molecules. From a.c. impedance spectroscopy, it has been shown that the ionic conductivities of the nanocomposite gel polymer electrolytes increase with increase in clay loading and exhibit a maximum value of 2.3×10^{-3} S cm^{-1} at room temperature for a 4 wt.% clay loading. This behaviour has been attributed to the higher uptake of liquid electrolytes by the nanocomposites. The presence of high dielectric constant clay layers also helps to dissolve more lithium salt ($LiClO_4$) by disturbing the charge environment of the electrolyte systems and this, in turn, facilitates higher ion conduction. The addition of MMT clays to PVdF not only reduces the interfacial resistance with lithium electrode but also provides a better electrochemical stability window of 4.6 V.

Acknowledgements

The authors are grateful to Mr. R. Gogoi for help in the synthesis of the polymer nanocomposites. Authors also thank Mr. A.K. Nath, Department of Physics, Delhi University for assistance with TEM studies.

References

[1] J.M. Tarascon, M. Armand, Nature (London) 414 (2001) 359–367.
[2] J.-H. Ahn, G.X. Wang, H.K. Liu, S.X. Dou, J. Power Sources 119–121 (2003) 422–426.
[3] S. Zhang, J.Y. Lee, L. Hong, J. Power Sources 126 (2004) 125–133.
[4] P.A.R.D. Jayathilaka, M.A.K.L. Dissanayake, I. Albinsson, B.-E. Mellander, Solid State Ionics 156 (2003) 179–195.
[5] S. Ahmad, H.B. Bohidar, S. Ahmad, S.A. Agnihotri, Polymer 47 (2006) 3583–3590.
[6] A.M. Stephan, K.S. Nahm, Polymer 47 (2006) 5952–5964.
[7] E.P. Giannelis, Adv. Mater. 8 (1996) 29–35.
[8] P. Jeevanandam, S. Vasudevan, J. Phys. Chem. B 102 (1998) 4753–4758.
[9] H.-W. Chen, T.-P. Lin, F.-C. Chang, Polymer 43 (2002) 5281–5288.
[10] M. Wang, F. Zhao, Z. Guo, S. Dong, Electrochim. Acta 49 (2004) 3595–3602.
[11] H.J. Walls, M.W. Riley, R.R. Singhal, R.J. Spontak, P.S. Fedkiw, S.A. Khan, Adv. Funct. Mater. 13 (2003) 710–717.
[12] T. Lan, P.D. Kaviratna, T.J. Pinnavaia, Chem. Mater. 6 (1994) 573–575.
[13] H.-L. Tyan, Y.-C. Liu, K.-H. Wei, Chem. Mater. 11 (1999) 1942–1947.
[14] Z. Wang, T.J. Pinnavaia, Chem. Mater. 10 (1998) 3769–3771.
[15] J.W. Gilman, C.L. Jackson, A.B. Morgan, R. Hayyis Jr., E. Manias, E.P. Giannelis, M. Wuthenow, D. Hilton, S.H. Phillips, Chem. Mater. 12 (2000) 1866–1873.
[16] L. Priya, J.P. Jog, J. Polym. Sci. B: Polym. Phys. 41 (2003) 31–38.
[17] Y.M. Song, Z.D. Zhao, W.X. Yu, B. Li, X.F. Chen, Sci. China B: Chem. 50 (2007) 790–796.
[18] S. Yu, W. Zheng, W. Yu, Y. Zhang, Q. Jiang, Z. Zhao, Macromolecules 42 (2009) 8870–8874.
[19] P. Martins, J.S. Nunes, G. Hungerford, D. Miranda, A. Ferreira, V. Sencadas, S. Lanceros-Méndez, Phys. Lett. A 373 (2009) 177–180.
[20] L. Wenhua, Z. Guangjie, Forest. Stud. China 6 (2004) 54–62.
[21] R. Delhez, T.H. de Keijser, J.I. Langford, D. Louer, E.J. Mittemeijer, E.J. Sonneveld, in: R.A. Young (Ed.), The Reitveld Method, Oxford University Press, Oxford, 1996, p. 132.
[22] G.K. Williamson, W.H. Hall, Acta Metall. 1 (1953) 22–31.
[23] A.M. Stephan, R. Thirunakaran, N.G. Renganathan, V. Sundaram, S. Pitchumani, N. Muniyandi, R. Gangadharan, P. Ramamoorthy, J. Power Sources 81–82 (1999) 752–758.
[24] M. Deka, A. Kumar, Electrochim. Acta 55 (2010) 1836–1842.
[25] F. Croce, L. Persi, B. Scrosati, F. Serraino-Fiory, E. Plichta, M.A. Hendrickson, Electrochim. Acta 46 (2001) 2457–2461.
[26] M.M.E. Jacob, E. Hackett, E.P. Giannelis, J. Mater. Chem. 13 (2003) 1–5.
[27] S.H. Chung, Y. Yang, L. Persi, F. Croce, B. Scrosati, E. Plichta, J. Power Sources 97 (2001) 644–648.
[28] M. Wang, S. Dong, J. Power Sources 170 (2007) 425–432.
[29] H. Xie, Z. Tang, Z. Li, Y. He, Y. Liu, H. Wang, J. Solid State Electrochem. 12 (2008) 1497–1502.
[30] L. Fan, Z. Dang, C.-W. Nan, M. Li, Electrochim. Acta 48 (2002) 205–209.
[31] D. Saikia, A. Kumar, Eur. Polym. J. 41 (2005) 563–568.
[32] V. Gentili, S. Panero, P. Reale, B. Scrosati, J. Power Sources 170 (2007) 185–190.
[33] S. Rajendran, O. Mahendran, R. Kannan, Mater. Chem. Phys. 74 (2002) 52–57.
[34] D. Saikia, A. Kumar, Electrochim. Acta 49 (2004) 2581–2589.
[35] S. Rajendran, O. Mahendran, T. Mahalingam, Eur. Polym. J. 38 (2002) 49–55.
[36] A.M. Stephan, Y. Saito, Solid State Ionics 148 (2002) 475–481.
[37] C.H. Parka, D.W. Kimb, J. Prakash, Y.-K. Sun, Solid State Ionics 159 (2003) 111–119.
[38] G. Vijayakumar, S.N. Karthick, A.R. Sathiya Priya, S. Ramalingam, A. Subramania, J. Solid State Electrochem. 12 (2008) 1135–1141.
[39] J. Song, Y. Wang, C.C. Wan, J. Power Sources 77 (1999) 183–197.
[40] M. Deka, A.K. Nath, A. Kumar, J. Membr. Sci. 327 (2009) 188–194.